QCD ASPECTS OF W/Z PRODUCTION AT THE TEVATRON

G. GUGLIELMO
University of Oklahoma,Norman,
OK 73109, USA
(For the CDF and DØ Collaborations)

Hadron colliders are providing valuable opportunities for studying the influence of the strong force on electroweak interactions in both the perturbative and non-perturbative regions. At the Fermilab Tevatron, analysis by CDF and DØ of $p\overline{p} \rightarrow W/Z + X$ events at $\sqrt{s} = 1.8$ TeV have been used to test a variety of leading order and next-to-leading order QCD predictions. Among the many promising benefits are improvements of parton distribution functions at high Q^2, demonstration of soft gluon radiation patterns which survive hadronization, and tests of perturbative QCD and resummation calculations.

1 W Charge Asymmetry

The W charge asymmetry as a function of rapidity (y) is sensitive to the ratio of u and d quark momentum distributions. $W^+(W^-)$ bosons are mainly produced in $p\overline{p}$ collisions through interactions of $u\overline{d}(d\overline{u})$ quarks. On average, the $u(\overline{u})$ quarks carry a larger fraction of momentum than the $d(\overline{d})$ quarks in a proton (antiproton). Therefore, the W^+ will usually experience a boost along the initial proton's momentum direction, while the W^- will generally be boosted along the antiproton's momentum direction. The difference in average boost direction between the W^+ and W^- bosons produced in $p\overline{p}$ interactions generates a measurable charge asymmetry as a function of y. With $\sqrt{s} = 1.8$ TeV at the Tevatron, the W charge asymmetry provides a valuable means of measuring the ratio of u to d quark distributions at low x ($0.006 < x < 0.34$) and high momentum transfer ($Q^2 \approx M_W^2$) where nonperturbative effects are minimal.[1]

The momentum along the beamline of the neutrino produced in a leptonic decay of the W boson is not determined experimentally. Therefore instead of measuring the charge asymmetry as a function of W rapidity, the asymmetry is measured as a function of the rapidity of the charged decay lepton ($l^{\pm}$). The asymmetry for the $l^{\pm}$ is modified (reduced) due to the $V - A$ nature of the electroweak decay. If the acceptances and efficiencies for detecting both l^+ and l^- are the same, the asymmetry can be written as:

$$A(y_l) = \frac{dN_{l^+}/dy_l - dN_{l^-}/dy_l}{dN_{l^+}/dy_l + dN_{l^-}/dy_l} \tag{1}$$

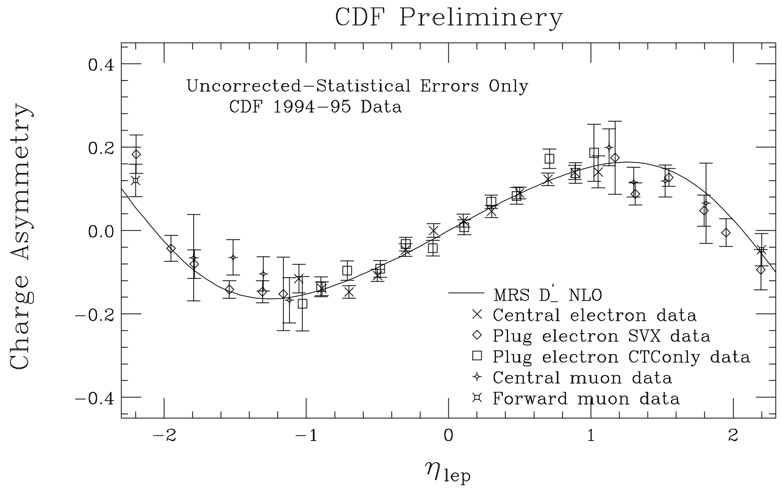

Figure 1: The CDF W charge asymmetry measurement as a function of rapidity before corrections were applied.

where $dN_{l^+}/dy_l(dN_{l^-}/dy_l)$ is the number of leptons $l^+(l^-)$ at a given lepton rapidity; the acceptance, efficiencies, and luminosity cancel. In addition, CP invariance requires that the asymmetry at y_l be equal and opposite to the the asymmetry at $y_l' = -y_l$. Therefore the asymmetries at equal but opposite y_l can be combined to reduce the effects of any differences in efficiencies for detecting the oppositely charge leptons.

The CDF data comes from 20pb^{-1} and 91pb^{-1} from the 1992-1993 and 1994-1995 collider runs respectively for both the electron and muon channels. The latter run greatly increases the data at forward rapidity and extends the rapidity range [2] over the earlier published results [1].

The direction of curvature of charged tracks in the CDF detector due to the magnetic field allows for the determination of the charge of the particle which made the track. The transverse energy of the lepton (E_T^l), and the missing transverse energy ($\not{E}_T$) of the event are both required to be greater than 25 GeV. The electrons are required to have $\mid y_e \mid < 1.1$ or $1.1 < \mid y_e \mid < 2.4$. The muons were required to be in the muon tracking system ($\mid y \mid < 1.0$), which was extended to $1.9 < \mid y_\mu \mid < 2.5$ in the forward region for the 1994-1995 run. Additionally, a requirement of no jets with ${E_T}^{Jet} > 30$ GeV was imposed to reduce the dijet background. Other quality cuts were also imposed.[1].

The new CDF preliminary results for the W charge asymmetry are shown (see Figure 1) compared to next-to-leading order (NLO) theory, calculated with

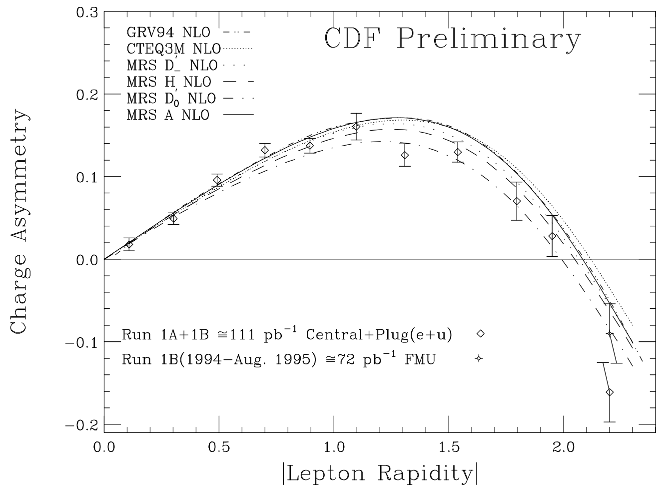

Figure 2: The corrected CDF W charge asymmetry as a function of rapidity folded about a rapidity of zero ($y = 0$). The total systematic errors for each bin are plotted on the x-axis.

the DYRAD [3] Monte Carlo, using various parton distribution functions (pdfs) from both the CTEQ[4] and MRS[5] families, unfolded in rapidity. Figure 2 shows the W charge asymmetry with asymmetries at equal and opposite rapidities combined. The differences between theory and data in the forward rapidity region indicates that the d/u quark ratio embodied in the pdfs may need to be adjusted. Constraints on the W charge asymmetry from the CDF data are already reducing the systematic error on measurements of the W mass due to pdfs.

2 Color Coherence in $W+$ Jets

Color coherence is the interference of color connected partons on soft gluon radiation. In jet events produced by a hard scatter, this interference can produce an angular distribution of particles which can be described using antennae patterns between the color connected partons involved.[6] Color coherence can take place in perturbative processes, where analytical calculations can be used to predict the effect, and in nonperturbative processes where phenomenological techniques must be used. In $p\overline{p} \rightarrow W+$ Jets interactions, the high Q^2 initial hard scatter can be analyzed with perturbative methods, while the low Q^2 fragmentation is in the nonperturbative regime and must rely upon phenomenology to describe the behavior.

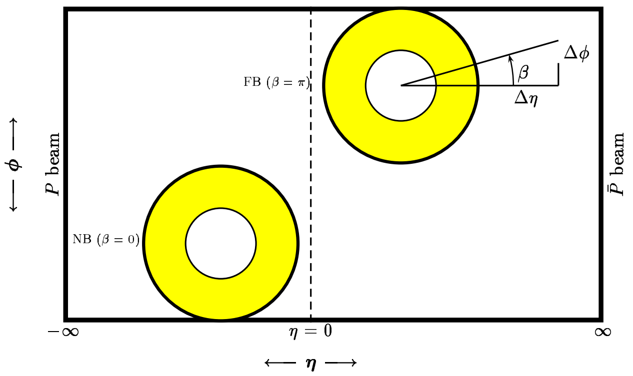

Figure 3: Diagram of the search regions in $\eta - \phi$ space for the color coherence measurement. The shaded areas show the regions used to map out the energy flow around the jet and the W boson on an event by event basis.

At the perturbative level, hard scattering at the parton level can involve the emission of soft gluons from the colored partons. The emitted gluons can also radiate soft gluons and soft $q\bar{q}$ pairs. The subsequent emissions can continue forming a cascade of soft partons in the event. This radiation can be modeled by Angular Ordering (AO) of the emitted soft gluons. Angular Ordering uses a monotonic increase (decrease) of the emission angle for successive soft gluons from incoming (outgoing) partons.[7]

At the nonperturbative level, color connections between the partons during the fragmentation process can affect the angular distribution of particles in the event. Different phenomenological models can be used to describe the fragmentation process. The Independent Fragmentation Model [8–9] doesn't account for color connections between partons involved in the shower process, while the Lund String Fragmentation Model [10] does.

In $W+$ Jets interactions, the angular distribution of soft gluons about the colorless W boson is expected to be nearly uniform, while the distribution around the jet is expected to have structure due to the color connections between the beam and the partons in the jet. These effects can be studied by searching in an annular region about the W or the jet in the η-ϕ (pseudorapidity and azimuthal angle) plane (see Figure 3). Any point in the annulus can be described by radius $R = \sqrt{\Delta\eta + \Delta\phi}$, where $\Delta\eta$ and $\Delta\phi$ are the separations between the point and the W (or jet) in η and ϕ. In addition to the radial separation, it is also important to know the angular separation from the plane defined by the beam axis (parallel to direction of initial partons and colored beam fragments) and the jet axis. The variable β, where $\tan(\beta) = sign(\eta)\Delta\phi/\Delta\eta$, is used for this purpose, with $\beta = 0$ pointing towards the beam nearest the W (or jet). Because of the symmetry expected in the distributions, each annulus can also be folded over along the line between $\beta = 0$ and π to increase statistics. Theory predicts that the pattern produced by dividing the distribution of soft gluon radiation around the jet by the distribution around the W, as a function of β, will show a relative depletion around $\beta = \frac{\pi}{2}$ with respect to $\beta = 0$ or π. An analytic calculation (Khoze and Stirling) [6], using color antennae radiation patterns, of the particle distribution around the jet divided by the distribution around the W is shown in the upper left plot of Figure 4. The calculation does not include soft particles from the underlying event which are expected to be more isotropic around both the jet and the W, and thus reduce the overall normalization of the divided distributions. Also the theory prediction does not include detector effects which may also effect the distributions.

DØ has analyzed $W \to e\nu$ events with jets from the 1994-1995 collider run. The event selection criteria include $E_T^e > 25$ GeV, $\mid y_W \mid < 0.7$, $\not{E}_T > 25$ GeV, $E_T^{Jet} > 10$ GeV and $\mid \eta_{Jet} \mid < 0.7$ (based on $R = 0.7$, fixed cone algorithm). In addition, a loose $\Delta\phi$ cut ($\frac{\pi}{2} < \mid \phi_W - \phi_{Jet} \mid < \frac{3\pi}{2}$) was imposed to reduce overlap between the annular regions around the jet and the W boson. Each annulus had an inner radius of 0.7 and an outer radius of 1.5. The search was performed by counting calorimeter towers with $E_T > 250$ MeV.

Three Monte Carlo samples were generated, with different levels of color coherent processes, using the PYTHIA 5.7 [11] program and passed through a full detector simulation. The first sample used Angular Ordering and the Lund String Fragmentation and is expected to have more color coherent effects than the other two sets. The second set used the Lund String Fragmentation but did not use Angular Ordering. The third set used Independent Fragmentation and did not use Angular Ordering, and thus represents a sample with no color coherence effects. The Monte Carlo events were reconstructed and required to pass the same basic requirements as the data.

The distribution of towers around the jet were divided by the distribution around the W for each sample, like the data, so that a shape comparison between Monte Carlo and data could be performed. Figure 4 has three plots showing the data overlayed with each of the three Monte Carlo samples, where the Monte Carlo has been normalized to the data. Figure 5 shows plots of data divided by each of the Monte Carlo samples and demonstrates more clearly the better agreement as a function for β between the data and the Monte Carlo sample with Angular Ordering and String Fragmentation.

Another way of quantifying the color coherence signal is to divide the average multiplicity at $\beta = 0$ by the average multiplicity at $\beta = \frac{\pi}{2}$. This should

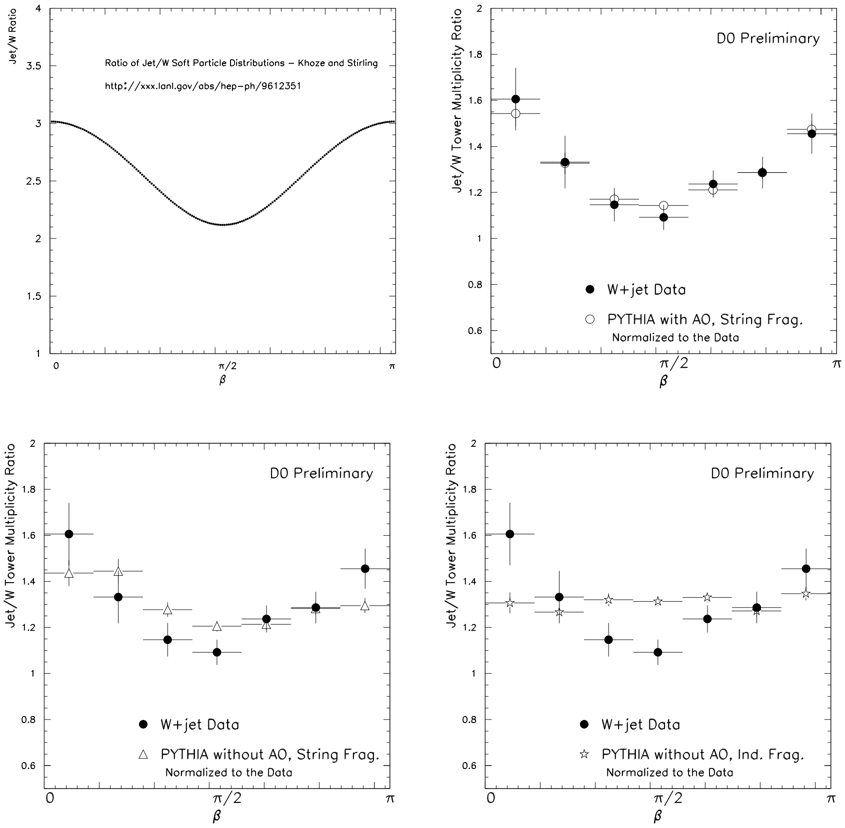

Figure 4: An analytic calculation, (upper left). of the soft particle distribution from a color antennae model. The DØ Tower multiplicity as a function of β is compared to: PYTHIA with String Fragmentation and Angular Ordering (upper right); PYTHIA with String Fragmentation and no Angular Ordering (lower left); PYTHIA with Independent Fragmentation and no Angular Ordering (lower right).

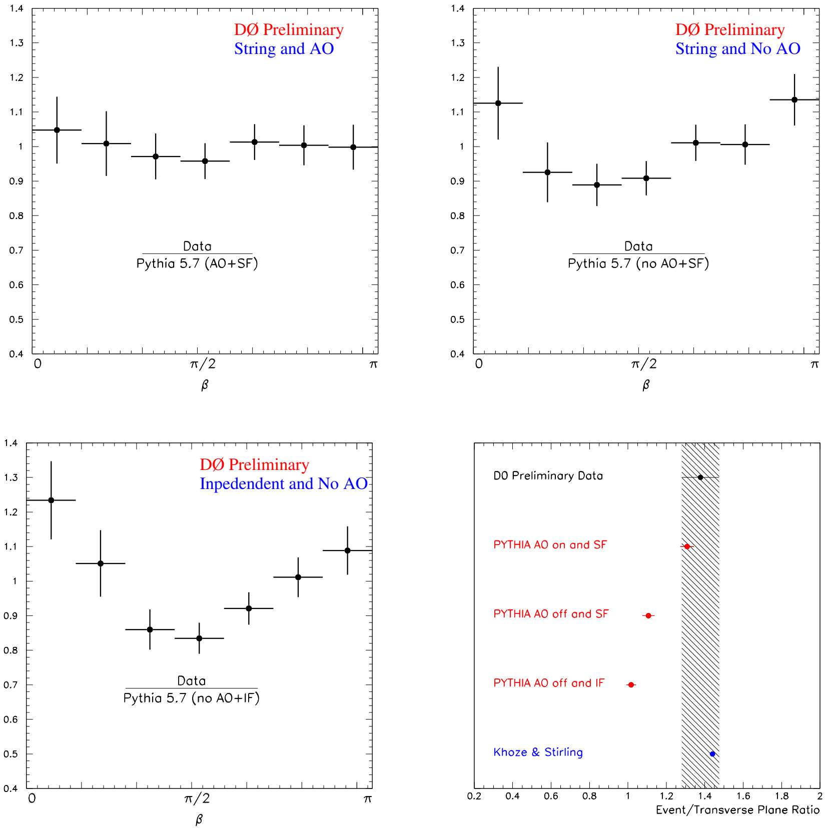

Figure 5: The DØ Tower multiplicity compared to Monte Carlo and theory. The upper left, upper right and lower left plots show the difference between data and theory divided by theory as a function of β for: PYTHIA with String Fragmentation and Angular Ordering (upper left); PYTHIA with String Fragmentation and no Angular Ordering (upper right); PYTHIA with Independent Fragmentation and no Angular Ordering (lower left). The ratio of average tower multiplicities for $\beta = 0$ and $\beta = \frac{\pi}{2}$ $(N^{ave}(\beta = 0)/N^{ave}(\beta = \frac{\pi}{2}))$ for the data, an analytic calculation, and three Monte Carlo samples (lower right).

magnify any color coherence effects by dividing the bin with the maximum expected relative multiplicity by the bin with the minimum expected relative multiplicity. In the lower right plot of Figure 5 this ratio has been plotted for the data, the analytic calculation using color antennae, and the three Monte Carlo samples. Both the analytic calculation and the Monte Carlo sample with Angular Ordering and Lund String Fragmentation agree very well with the data. The other two Monte Carlo samples, with less or no color coherence effects included, do not agree with the data.

3 $W/Z+$ Jets

The production of $W/Z+$ Jets events in $p\overline{p}$ collisions provides an important test of QCD calculations because of the high $Q^2 \approx M^2_{W/Z}$ involved. The analyses of CDF and DØ provide a good complementary set of results for studying the perturbative calculations involved. DØ results on the ratio of exclusive $W+1$ Jet to $W+0$ Jets as a function of the minimum jet E_T is compared to NLO theory. CDF has inclusive $W+\geq N$ Jets and $Z+\geq N$ Jets cross section results which are compared to leading order (LO) theory.

The DØ analysis counts the number of events with zero jets above a minimum E_T threshold (E_T^{min}) and the number of events with exactly one jet above the threshold. The second value can then be divided by the first to yield the desired ratio. Systematic effects common to both $W+0$ and $W+1$ Jets, like the uncertainty on the luminosity, cancel out in the ratio. The original motivation for this measurement was to try measuring the strong coupling constant α_s. The ratio can be written at NLO as:

$$R^{10}(E_T^{min}, \Delta R) = \alpha_s \frac{(A_1^{W1} + \alpha_s A_2^{W1})}{(A_0^{W0} + \alpha_s A_1^{W0})} \tag{2}$$

The ratio is sensitive to the pdfs, which are sensitive to α_s through the evolution of the equations and this effect seems to cancel the hard scatter sensitivity. While this ratio turns out to be not very sensitive to α_s at $\sqrt{s} = 1.8$ TeV, in sharp contrast to the strong dependence seen at $\sqrt{s} = 630$ GeV, it does allow for a good test of NLO calculations.

76pb^{-1} of data collected during the 1994-1995 collider run were used in this analysis. The electron was required to have $E_T^e > 25$ GeV, $|\,\eta\,| < 1.0$ and be isolated. The event was required to have $\not{E}_T > 25$ GeV. Jets were formed on a cone of $R = 0.7$ using a fixed cone algorithm. The number of jets with E_T above E_T^{min}, which was varied between 20 GeV and 60 GeV, were counted. Other quality requirements were imposed on each event.

The background for these events was studied as a function of $\not{E}_T$ by comparison with an unbiased trigger sample. In the very low $\not{E}_T$ region, below 10 GeV, the data are expected to be almost completely due to background from multijet events. Normalizing the distributions in this low $\not{E}_T$ region allows for the background shape and size to be determined at higher values of $\not{E}_T$. This method was used to estimate the dominant background and separately correct the $W+0$ and $W+1$ jets samples. Additional backgrounds were determined from ISAJET [12] Monte Carlo and a simulation of the detector. The samples also were corrected for electron efficiencies that would not cancel in the ratio.[13] Nowadays, the efficiency determination and the jet energy scale dominate the error. Of the 36984 $W \rightarrow e\nu$ events, 33617 had zero jets and 2829 had 1 jet with jet $E_T^{min} = 25$ GeV.

The NLO theory was calculated using DYRAD [3] with various pdfs from the MRSA [5] and CTEQ4 [14] families and renormalization scale (μ) of M_W. The E_T of the jets were smeared to account for detector resolution. In Figure 6 the ratio is plotted for both data and theory as a function of jet E_T^{min}. The upper plot shows a comparison to theory using MRSA' and CTEQ4M pdfs. The lower left and lower right plots show comparison to various pdfs from the CTEQ4 and MRSA families, demonstrating the range of predictions within a family. The DYRAD NLO predictions showed little sensitivity when μ was varied between $M_w/2$ and $2M_W$. The plots of R^{10} as a function of jet E_T^{min} show the NLO theory is consistently lower than the data.

CDF has measured the cross sections for $W+\geq N$ Jets and $Z+\geq N$ Jets from the 1992-1995 collider run. The $W \rightarrow e\nu$ sample [15] consists of 108pb^{-1} of data and the $Z \rightarrow ee$ sample, previously published [16], represents 106pb^{-1} of data. The W analysis required an electron of $E_T \geq 20$ GeV and $|\eta| \leq 1.1$, $\not{E}_T > 30$ GeV, and counted jets with $E_T > 15$ GeV and $|\eta| < 2.4$ based on a 0.4 cone size. The Z had the same basic electron requirements on the first electron. The second electron was required to have $E_T \geq 20$, 15, or 10 GeV and $|\eta| \leq 1.1$, $1.1 \leq |\eta| \leq 2.4$, or $2.4 \leq |\eta| \leq 3.7$ respectively. Also, the reconstructed electron pair mass was required to be within 15 GeV/c^2 of the nominal Z boson mass (91 GeV/c^2). Other quality requirements were imposed to reduce the background on both analyses. There were 51431 $W \rightarrow e\nu$ and 6708 $Z \rightarrow e\nu$ events.

The number of events with $W+\geq N$ Jets was corrected for efficiencies and backgrounds for each value of N. The $W+\geq N$ Jets cross sections were determined by multiplying the ratio of corrected events $(W+\geq N)/(W+\geq 0)$ by the CDF $W \rightarrow e\nu$ inclusive cross section of 2490 ± 120 pb.[17] The $W+\geq N$ Jets cross sections are listed in Table 1 along with the $Z+\geq N$ Jets cross sections.

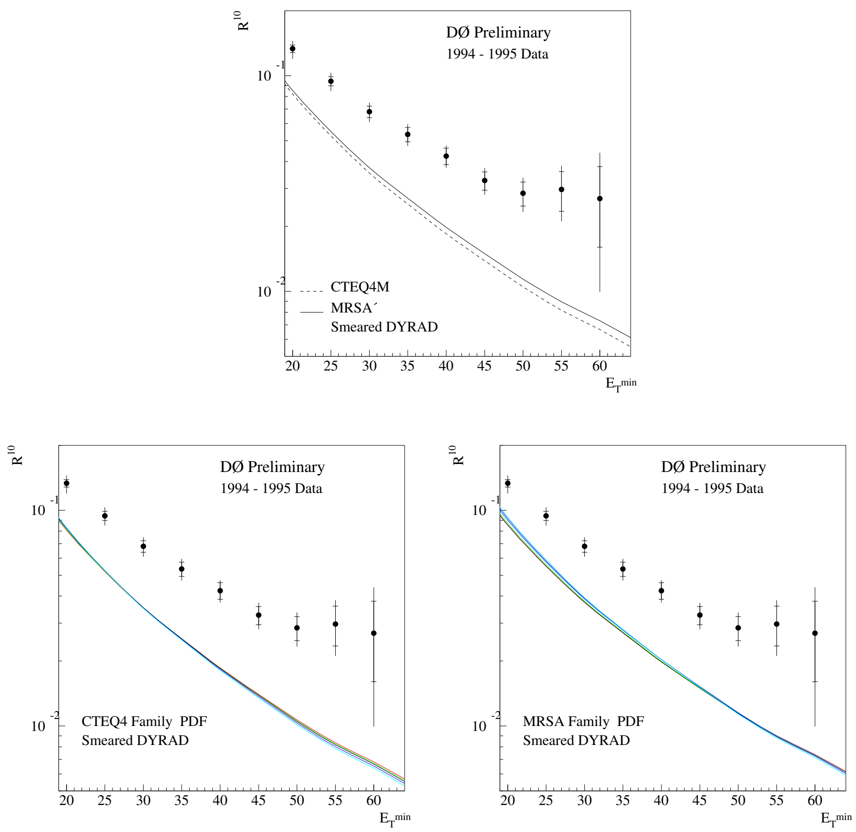

Figure 6: The DØ $(W + 1 \text{ Jet})/(W + 0 \text{ Jets})$ as a function of jet E_T^{min} compared to the smeared DYRAD predictions. Comparison to smeared predictions (upper plot) using MRSA' (solid line) and CTEQ4M (dashed line) pdfs. Comparison to the smeared predictions using the CTEQ4 family (lower left) and MRSA family (lower right) pdfs. The renormalization scale was $\mu^2 = M_W^2$. The inner error bars are statistical only, the outer error bars are statistical and systematic errors in quadrature.

Table 1: CDF $W/Z+\geq N$ Jets cross sections. Note that the $W+\geq 0$ Jets cross section is the CDF inclusive result from a previous measurement.

$W/Z+N$ Jets	$\sigma_W\cdot$BR (pb)	$\sigma_Z\cdot$BR (pb)
$N\geq 0$	$\equiv 2490\pm120$	$231\pm6\pm11$
$N\geq 1$	$471\pm5.4\pm57$	$45.2\pm1.2\pm5.7$
$N\geq 2$	$101\pm2.4\pm19$	$9.7\pm0.6\pm1.8$
$N\geq 3$	$18.4\pm1.1\pm5.2$	$2.03\pm0.28\pm0.49$
$N\geq 4$	$3.1\pm0.6\pm1.3$	$0.43\pm0.13\pm0.11$

The leading order QCD predictions for the $W/Z+\geq N$ Jets cross sections were generated using the VECBOS [18] Monte Carlo program. In order to account for gluon radiation and parton fragmentation effects, the HERWIG [19] shower simulation was used. The output of the combined VECBOS and HERWIG Monte Carlo was then processed through the CDF detector simulation. The CTEQ3M [20] pdf along with two different renormalization scales were used. A comparison of the cross section results with the Monte Carlo are shown in Figure 7. Both the W and Z plus jets cross sections show the same trends when compared to theory. The harder scale of $Q^2 = M^2_{W/Z} + (P_T^{W/Z})^2$ is roughly 1.7 times lower than the data from $N = 1$ up to $N = 4$. The softer scale of $Q^2 = \langle P_T \rangle^2$ of the partons is slightly higher than the data for $N = 2$ through $N = 4$, but is lower for $N = 1$ and only the $N = 1$ result is not covered by the theory band. In Figure 8 the jet E_T for the four highest E_T jets is plotted along with the LO theory prediction described above with $Q^2 = \langle P_T \rangle^2$ of the partons. The theory is normalized to the data so that a shape comparison of the E_T spectrum could be performed. The normalized theory agrees well with the data over a wide range in E_T, indicating that theory does a reasonable job of describing the shape of the E_T spectra.

4 P_T of W and Z Bosons

Measurement of the P_T of W and Z bosons produced in $p\overline{p}$ interactions provides a means of testing resummation techniques at low P_T and perturbative QCD at high P_T. DØ has analyzed 12.4pb^{-1} of data from the 1992-1993 collider run to measure the P_T^W spectrum. In a complimentary analysis, DØ has measured the P_T^Z spectrum from 97pb^{-1} of data collected during the 1994-1995 run. The $W \rightarrow e\nu$ sample represents 10112 events, and there are 4006 events in the $Z \rightarrow ee$ sample. Despite having many more events in the W sample, the

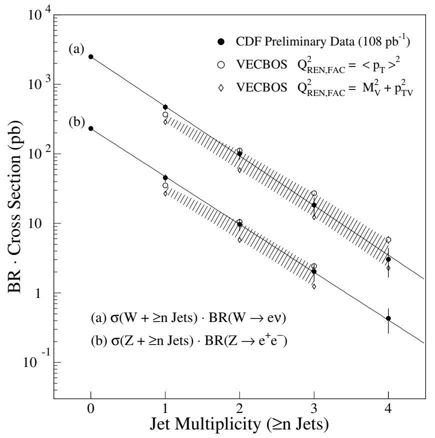

Figure 7: The CDF $W/Z+\geq N$ Jets cross sections compared to VECBOS plus HERWIG (for gluon radiation and fragmentation) as a function of number of jets in the event.

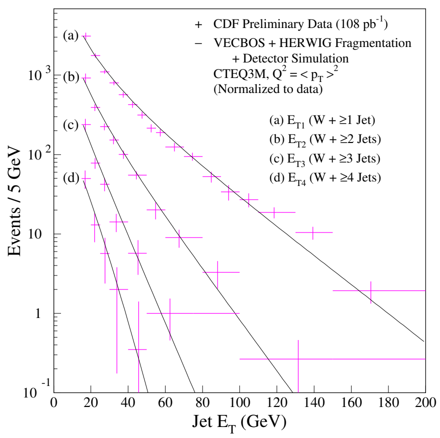

Figure 8: The CDF jet E_T distributions, for jets in $W+$ Jets events, cross sections compared to VECBOS plus HERWIG (for gluon radiation and fragmentation) as a function of number of jets in the event. The errors include both statistical and background subtraction contributions.

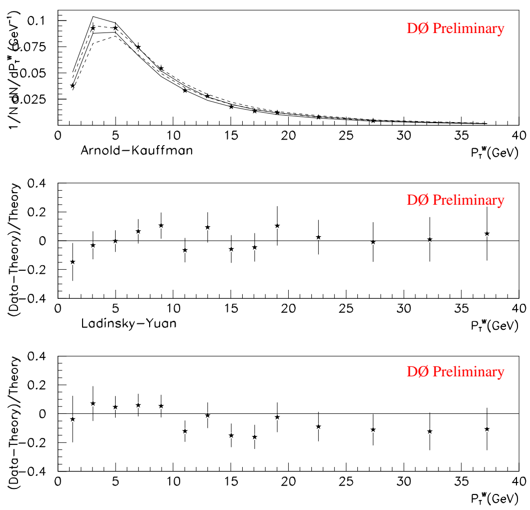

Figure 9: The DØ P_T^W distribution compared to theory in the low P_T region. The top plot shows the data (stars) compared to NLO plus Resummation (solid lines, Arnold and Kauffman) and LO plus Resummation (Ladinsky and Yuan) using the MRSA pdf. The middle plot shows the normalized difference between data and theory divided by the normalized theory (Arnold and Kauffman). The bottom plot shows the normalized difference between data and theory divided by the normalized theory (Ladinsky and Yuan).

Z sample provides a stronger test of the theory due to the better resolution in measuring electrons compared to neutrinos. Another difference between the two measurements arises because DØ cannot experimentally separate the Drell-Yan electron pairs (produced by γ^* exchange) from those produced from Z bosons. Therefore, the P_T measurement for Z bosons actually refers to the P_T of electron pairs from both Z and Drell-Yan production combined.

The W analysis required an electron of $E_T > 25$ GeV, and either $|\eta| < 1.0$ or $1.5 < |\eta| < 2.5$. There was an $\not{E}_T > 30$ GeV requirement and any event with a second electron having $E_T > 20$ GeV was rejected. The Z analysis required one electron of $E_T > 25$ GeV, and $|\eta| < 1.0$. The second electron had the same E_T requirement of 25 GeV, but was allowed to either have $|\eta| < 1.0$ or $1.5 < |\eta| < 2.5$. There is also a requirement that the reconstructed electron pair mass be within a ± 15 GeV$/c^2$ window around the nominal Z boson mass (91 GeV$/c^2$). Additional quality cuts were imposed on the samples.[21]

Both analyses measure the cross section as a function of P_T. The cross

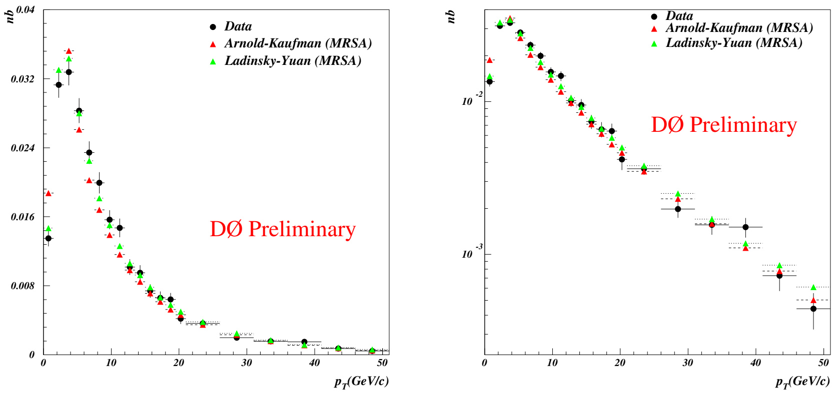

Figure 10: The DØ P_T^Z distribution (circles) compared to NLO plus Resummation (Arnold and Kauffman) and LO plus Resummation (Ladinsky and Yuan), using the MRSA pdf in the theory.

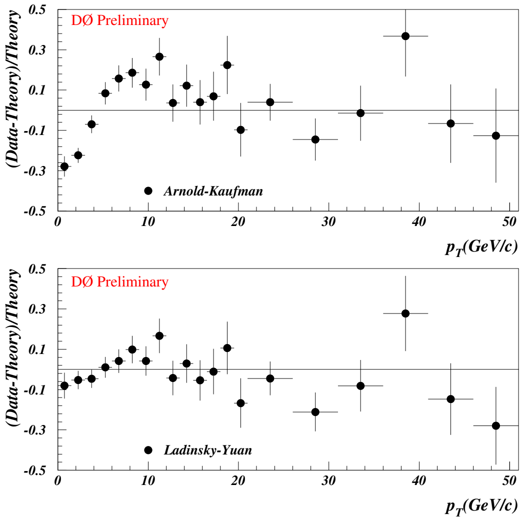

Figure 11: The DØ P_T^Z distribution compared to theory in the low P_T region. The upper plot shows the normalized difference between data and theory divided by the normalized theory (Arnold and Kauffman). The lower plot shows the normalized difference between data and theory divided by the normalized theory (Ladinsky and Yuan).

section as a function of P_T can be written as:

$$\frac{d\sigma}{dP_T}(i) = \frac{N_{obs}(i) - N_{bkg}(i)}{\epsilon(i)\Delta Bin(i) Br(e)\mathcal{L}} \tag{3}$$

where $N_{obs}(i)$, $N_{bkg}(i)$, $\epsilon(i)$, and $\Delta Bin(i)$ are the number of observed events, number of expected background events, efficiency, and P_T bin width for the ith P_T bin. $Br(e)$ and $\mathcal{L}$ are the branching fraction to the electron channel and the luminosity respectively. From this equation, the cross section as a function of P_T was determined. The Monte Carlo W and Z P_T spectra were generated using a fast Monte Carlo program.[22] This simulation is used to produce smearing effects in the theoretical predictions for comparison to the data. The MRSA pdf was used for both analyses. Two sets of theoretical P_T spectrums were generated and smeared. The first was a combination of resummation techniques, for low P_T, and NLO perturbative calculations, for the high P_T with a matching between the two at moderate P_T (Arnold and Kauffman).[23] The second also used resummation and matching, only this time the perturbative calculation was LO and went out to only 50 GeV in P_T (Ladinsky and Yuan).[24]

The W cross section distributions for theory and data were normalized to unity. Fig. 9 is a comparison for the low P_T region for both of the theories and the data. The Z cross section distribution for the low P_T region out to 50 GeV is shown in Figures 10-11 where the theory has been normalized to the data. In the low P_T region, both the W and the Z measurements seem to be described fairly well by at least one of the theories.

5 Summary

CDF results on the W charge asymmetry indicate the d/u quark ratio in pdfs may need tuning. The color coherence results from DØ in $W+$ Jets events are best described by Monte Carlo using String Fragmentation and Angular Ordering. In addition, the analytic calculation using color radiation patterns by Khoze and Stirling is in agreement with the DØ color coherence data. NLO theory at $Q^2 = M_W^2$ is consistently lower than the DØ R^{10} results. Also, LO theory is lower than the CDF results for $W/Z+ \geq N$ Jets at $Q^2 = M_{W/Z}^2 + (P_T^{W/Z})^2$ and $N > 0$. Finally, the $P_T^{W/Z}$ results from DØ show that Resummation calculations do a fairly good job of describing the P_T spectrum in the low P_T region for both the W and Z bosons.

Acknowledgments

We are grateful to the DØ and CDF collaborations for discussions of their data.

References

1. F. Abe, *et al.*, (CDF Collaboration), *Phys. Rev. Lett.* **74**, (1995).
2. A. Bodek, FERMILAB-Conf-96/341-E.
3. W. Giele, *et al.*, *Nucl. Phys.* B **403**, 633 (1993).
4. J. Botts, *et al.*, *Phys. Lett.* B **304**, 159 (1993).
5. A.D. Martin, *et al.*, RAL-93-077; RAL-94-055.
6. V.A. Khoze and W.J. Stirling, hep-ph/9612351.
7. S. Abachi, *et al.*, (DØ Collaboration), FERMILAB-Conf-95/182-E.
8. A. Krzywicki, *et al.*, *Phys. Rev.* D **6**, 924 (1972).
9. J. Finnkelstein and R.D. Peccei, *Phys. Rev.* D **6**, 2606 (1972).
10. B. Andersson, *et al.*, *Z. Phys.* C **20**, 317 (1983).
11. T. Sjöstrand, Comput. Phys. Commun. *82*, 74, (1994).
12. F.E. Paige and S.D. Protopopescu, "Isajet Manual", Brookhaven National Laboratory, Upton, New York (1992).
13. T.M. Joffe-Minor, "A Measurement of the Ratio of Production Cross Sections for $W + 1$ Jet to $W + 0$ Jets at $\sqrt{s} = 1800$ GeV", Ph.D. Thesis, (1997).
14. H.L. Lai *et al.*, *Phys. Rev.* D **55**, 1280 (1997).
15. J.R. Dittmann *et al.*, CDF/PUB/JET/PUBLIC/4179.
16. F. Abe *et al.*, (CDF Collaboration), *Phys. Rev. Lett.* **77**, 448 (1996) .
17. F. Abe *et al.*, (CDF Collaboration), *Phys. Rev. Lett.* **76**, 3070 (1996).
18. F.A. Berends *et al.*, *Nucl. Phys.* B **357**, 32 (1991).
19. G. Marchesini and B. Webber, *Nucl. Phys.* B **310**, 461 (1988).
20. H.L. Lai *et al.*, *Phys. Rev.* D **51**, 4763 (1995).
21. S. Abachi *et al.*, (DØ Collaboration), *Phys. Rev. Lett.* **75**, 1456 (1995).
22. E. Flattum, DØ Note 2397.
23. P. Arnold and R. Kauffman, *Nucl. Phys.* B **349**, 381 (1991).
24. G.A. Ladinsky and C.P. Yuan, *Phys. Rev.* D **50**, 4239 (1994).